Received: 24 April 2023 | Revised: 17 August 2023 | Accepted: 27 August 2023

IET Quantum Communication

DOI: 10.1049/qtc2.12071

ORIGINAL RESEARCH

Modelling and experimental testing of an optical synchronisation beacon designed for high-loss satellite quantum communication

Peide Zhang[1] | David Lowndes[1] | Milan Stefko[1] | Daniel Oi[2] | John Rarity[1]

[1]Department of Engineering, University of Bristol, Bristol, UK

[2]SUPA Department of Physics, University of Strathclyde, Glasgow, UK

Correspondence

Peide Zhang.
Email: peide.zhang@bristol.ac.uk

Funding information

Engineering and Physical Sciences Research Council, Grant/Award Numbers: EP/T001011/1, EP/T517288/1; UK Space Agency, Grant/Award Number: NSTP3-FT2-065; Chinese Government Scholarship, Grant/Award Number: 201906840125

Abstract

Long-distance free space quantum key distribution based on CubeSats can be used to establish global quantum secure communication networks, with potential commercial applications benefitting from the low cost of its design and launch. Detecting single-photon level optical pulses sent from space requires highly accurate and robust timing systems to pick out signals from the noise. For such high-loss applications, we envisage a low-repetition (sub-MHz) beacon laser emitting short (ns) high-peak-power pulses from which interpolated quantum signal arrival windows can be derived. We firstly study theoretically the effects of jitter on the efficiency of gating quantum signals including all important jitter sources, and then experimentally investigated it by changing the clock jitter, and the result shows that the greater jitter will reduce the gating rate of the signal. The experimental interpolation error is tested against loss under laboratory conditions giving results close to our model. We also found that the jitter introduced by the Doppler effect can be ignored with a repetition rate larger than 1 kHz. This model can be directly used for the performance analysis and optimisation of all quantum and non-quantum systems using similar synchronisation schemes over terrestrial free space or fibre.

KEYWORDS

quantum communication, quantum cryptography

1 | INTRODUCTION

In response to the threat to existing cryptographic systems posed by the development of quantum computers, quantum key distribution (QKD) technology has made great strides in the past 2 decades, and QKD systems using optical fibres as the channel have even moved from the laboratory to the commercial stage. However, the signal power in optical fibres undergoes exponential attenuation at a rate of about 0.2 dB/km, which greatly limits its code rate and communication distance to less than 600 km. In contrast, free space quantum communication has more potential in long-distance and mobile user situations, for instance, unmanned aerial vehicles, plane and satellite. In particular, the satellite is a promising platform to establish a global quantum communication network benefitting from it's stable long-term orbit and planet-wide optical visibility.

The launch and demonstration of the Micius satellite confirmed the possibility of deploying a satellite-based quantum communication systems and greatly increased people's interest in satellite-based quantum communication [1, 2]. However, establishing a stable optical link in free space is challenging, especially on a resource-limited platform like a satellite. The quantum beam will suffer high channel loss and relative motion between satellite and optical ground station (OGS), and the significant background light noise further worsens the signal noise ratio (SNR). To solve this, a classical beam (beacon) is utilised to synchronise the quantum signal

Abbreviations: APD, avalanche photodiodes; APT, acquisition, pointing, and tracking; FPGA, field programmable gate arrays; FWHM, full width half maximum; GPS, global positioning system; LEO, low earth orbit; NEP, noise equivalent power; OGS, optical ground station; PLL, phase-locked loops; PPS, pulse per second; PRBS, pseudorandom binary sequence; QKD, quantum key distribution; RLC, resistor, inductor and capacitor; RMS, root mean square; SNR, signal noise ratio; SPCM, single-photon counting module; SWaP, size, weight and power; TDC, time to digital convert; UAV, unmanned aerial vehicles; VOC, voltage controlled oscillator.

between the transmitter and receiver. A distinguishable and sharp pulse is required to identify and gate the corresponding quantum signal from the noisy background. On the other hand, the beacon needs to provide enough power and accurate divergence to point and track the OGS and also provide a stable polarisation reference to compensate the satellite rotation.

Several methods have been proposed to synchronise two sites in the QKD system. Performing cross-correlation on the key strings of the transmitter and receiver to achieve synchronisation is the most original way. It is very effective in a fibre-based QKD system as the fibre is naturally immune to Doppler, atmospheric effect and channel loss variation, which have significant effect in the free space scenario. Calderaro et al. proposed 'Qubit4Sync' which uses the histogram of time interval between two adjacent qubits to recover the periodic difference between the transmitter and receiver, but it cannot overcome the relative motion and random jitter introduced by atmosphere and channel loss [3]. Wang et al. demonstrate using quantum photon tags to analyse the centre frequency of a quantum signal train and then a method using this to compensate the Doppler effect [4]. Using stable enough high-precision clocks like atomic clocks is another way to sync two clocks. As a mature technology, they are often used in satellite-based navigation and communication systems. The high clock stability is on the level of 10^{-14} over one day, while the most recent report shows that the stability has been improved up to 4.7×10^{-15} at 10^4 s [5, 6]. However, deploying an atomic clock is complex with high cost and size requirement, which is not suitable for low-cost payload like micro-satellite or nano-satellite.

The most practical way considering the performance, cost and technology readiness is to transmit a bright classical optical pulse alongside the quantum signal and is widely used in the reported works. Micius combines a 160 mW bright laser and global positioning system (GPS) pulse per second (PPS), achieving a synchronisation jitter of 500 ps [1]. Wang et al. proposed a synchronisation modulation method which uses left-shift (bit-0) and right-shift (bit-1) related to a periodic pulse to modulate in pseudorandom binary sequence (PRBS) and to compensate the Doppler effect, which can achieve 200 ps precision under 10 dB loss [7]. Agnesi et al. used a laser ranging system to launch a 55 ps laser pulse to a satellite at a distance of 7500 km [8] achieving a detection accuracy of 230 ps of the reflected photons, but requires the co-location of the transmitter and receiver and an internal clock network to gate the detection signal as well as a known target distance. Zhang et al. proposed an encoding scheme based on a hybrid de Bruijn code which could directly decode the quantum signal index with high-loss tolerance and real-time synchronisation potential [9]. The newest work demonstrated by Berra also represents a synchronisation system using a bright laser, which is locked to the same master clock with a quantum signal [10]. However, achieving synchronisation using classical optical signals on a micro-nano-satellite platform can be difficult due to limited resources and device performance, parameter selection and environmental factors make obtaining a stable and reliable reference clock even more challenging. For a reference clock, the most important point is the synchronisation stability, and the parameter characterising this performance is the clock jitter. A severe jitter can cause a desynchronisation between the beacon and the quantum signal, which further leads to a decrease in the gating efficiency of the quantum signal, or even the failure to generate a secure key. Therefore, studying the effect of synchronous clock jitter on quantum key generation rates and the sources of clock jitter is important for the evaluation and optimisation of clock designs and the improvement of quantum detection efficiency.

We introduce a well-designed QKD system with timing and synchronisation modules built to verify the clock performance under different scenarios like changing channel length, Doppler effect, atmospheric effect and channel loss variation for the small satellite constrained by the SWaP. It is also the payload prototype for the various planned missions. We investigate the effect of jitter and the gating window on the efficiency of quantum detection. The jitter sources are analysed, the jitter contribution from the detector is modelled and the interpolation errors and the effects of Doppler are established. The model can be used to estimate the system timing performance, and more importantly, it can be used as a guidance for clock design optimisation to improve the efficiency of quantum detection. Although it is abstracted from the free space quantum communication system, it can be widely used in many optical systems either fibre- or free space-based including optical communications, quantum navigation, quantum clock transfer and some basic physics experiments [11].

2 | JITTER EFFECT ON QUANTUM KEY DETECTION

In a fibre-based QKD system, benefitting from the fixed-length channel, the processing typically synchronises the transmitted and received quantum signal by using stable clocks and comparing the string patterns of a sub-set of revealed bits. Mathematically, it cross-correlates the transmitted key string and the received key string to generate a correlation coefficient curve with one peak, and the peak position is exactly the time shift between the transmitted time domain and the received time domain. After shifting one of the string to align with the other, each transmitted and received pair can be identified, and the reconciliation process can proceed.

However, satellites-based QKD, while bringing the advantages of communication range, also brings problems. The relative movement of the two parties in the communication leads to the failure of the traditional reconciliation methods. The channel length changes during the communication due to satellite in-orbit position and, to a lesser extent, atmospheric refractive index. The time relationship between the received keys has various offsets relative to the transmitted sequence, and these offsets are usually non-linear and difficult to recover.

To address the above problem, we developed a downlink beacon emitting short high intensity pulses and encode the de Bruijn sequence onto it to carry absolute time coordinates relative to the transmitter time domain. The downlink beacon

is a bright classical laser beam used for coarser acquisition, pointing and tracking (APT) locking the OGS onto the moving satellite. Additionally, the polarisation of the received beacon provides a reference of the polarisation angle difference between the transmitter and receiver resulting from the spin of the satellite and the adjustment of the OGS pointing angle. The synchronisation sequence is linked in time with the quantum key so that the receiver can uniquely identify the quantum signal based on the decoding result of the beacon enabling time-gated raw key generation.

An ideal key gating process can be described by when a beacon pulse arrives and its timestamp is captured, find the same instant in the quantum string, and search if there is any captured event within the gated window centred on the timestamp of the beacon. All the found events will be registered as the quantum raw key, and others will be discarded, and each gated raw key bit will be marked with an index, which is the same as the corresponding beacon.

The practical scenario is much more complicated. Due to phase noise, signal amplitude variations and the Doppler effect, the beacon cannot be synchronised perfectly with the quantum signal, which makes it impossible to find the corresponding raw key accurately when gating. The uncertainty in the synchronisation is called timing jitter. Furthermore, thermal noise inside the devices, as well as background light can cause the single-photon counting module (SPCM) to detect many fake quantum signals, which are evenly distributed over the entire time scale and are also registered as desired signals during processing. Therefore, the impact of jitter and noise on system performance and the quantification, source and control of jitter are very important for the development and improvement of a QKD system.

Figure 1 shows how the jitter and noise floor affect the quantum raw key gating. The dash line shows the original pulse shape emitted from the source; most of the raw key can be gated when a gate window with a suitable width is applied, which is represented by the dot-dash line in the figure. Once the system introduces some noise like dark counts from the detector and background photons from the environment, the gated raw key will be mixed with some 'undesired' signal which will increase the quantum bit error rate. Worse still, when the signal suffers from jitter, the pulse width will increase, and the amplitude will decrease accordingly, resulting in a gate window of the same width only capturing fewer raw keys. An obvious approach would be to widen the gate to capture more photons, but this attempt would bring more noise into the selection range, thus degrading the signal-to-noise ratio. A simulation is demonstrated to figure out how the jitter affects the raw key gating specifically. It also can give some guidance about how to choose an optimum gate width balancing the gated detection efficiency and the SNR. The jitter and gate width effect on the performance is highly dependent on the actual signal pulse width, so all the jitter and gate widths will be quantified as a ratio of pulse widths. Considering the practical situation, the quantum pulse width is set to 1 ns, the maximum value of gate will not exceed two times the width of the signal and the maximum value of jitter will not exceed five times the width of the signal. Several parameters are defined here to qualify the performance of the system. The gating efficiency is the ratio between the number of gated raw key and the number of received raw key which could reflect the detection efficiency of the system. The noise ratio is the ratio between the noise count and total gated number within the gate window. The SNR is similar with the noise ratio, which could show the signal-to-noise level contrast, defined as the gated raw key number and the noise count.

Figures 2 and 3 show the simulation result of how the jitter will affect the gating efficiency and the noise ratio and how to choose a reasonable width value to maximise the system performance. In Figure 2, the trends show how the gating efficiency and noise ratio change as the jitter increases. The curves labelled LG correspond to the left Y-axis showing the gating

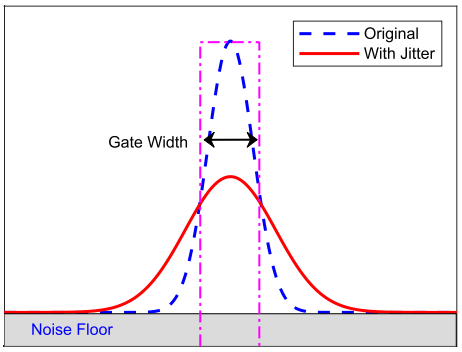

FIGURE 1 The comparison between the ideal pulse and the actual pulse which suffers from additional jitter and noise. The choice of gate width affects the efficiency of signal photon collection, while widening the gate brings more noise photons. Optimisation of the gate width requires a careful balance between efficiency and signal to noise, modelling the jitter as a Gaussian distributed variable mapped into a square time window.

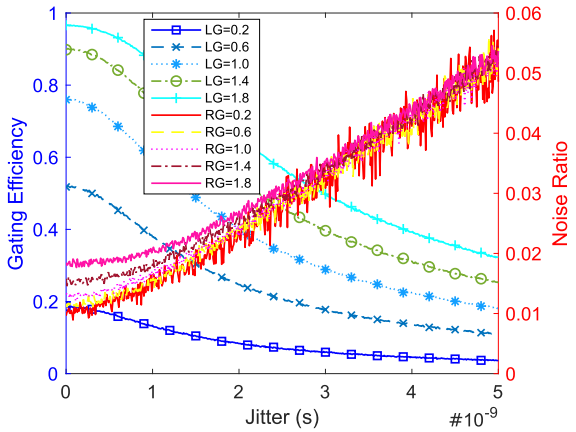

FIGURE 2 The raw key gating efficiency and noise ratio change as jitter is increased for a range of gate widths. The line with LG label is corresponding to the left Y-axis, while the line with RG label is corresponding to the right Y-axis. The values of LG and RG represent the ratio between the gate width and the pulse width. For example, the LG = 0.2 means that the gate width is 0.2 × the actual quantum pulse width. The quantum pulse width used in the simulation is 1 ns.

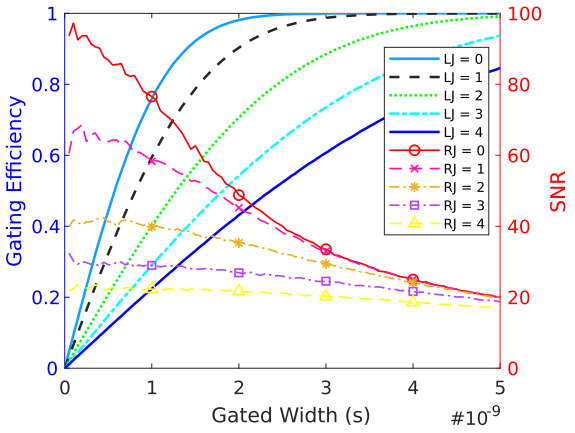

FIGURE 3 The raw key gating efficiency and signal noise ratio change with the gate window width increase under different jitters. The line with LJ label is corresponding to the left *Y*-axis, while the line with RJ label is corresponding to the right *Y*-axis. The LJ and RJ represent the ratio between the jitter and the quantum pulse width. The quantum pulse width used in the simulation is 1 ns.

efficiency change with the jitter. The lines labelled RG correspond to the right *Y*-axis and show how the noise ratio changes with the jitter. As the jitter increases, the gating efficiency goes down slowly when jitter is less than 1 and then drops in a Gaussian-like profile as jitterincreases. Additionally, the gating efficiency increases as the gate width becomes wider. At the point of jitter equal to 0, when the gate width is shorter than the pulse width, the gating efficiency saturates close to 100%, and most of the photons are located within the pulse width. However, once the jitter is larger than twice the pulse width, the gating efficiency increases roughly linearly with the wider gate width. For the noise ratio, a low jitter (<1 pulse width) noise ratio is not strongly affected but it increases roughly linearly for jitter >1 reflecting the fall in gating efficiency at a constant noise count. Once the jitter is greater than twice the pulsewidth, there is little change in the noise ratio as gate width is changed over the range investigated (0.2–1.8 × pulsewidth).

In Figure 3, the lines labelled as 'LJ' are the gating efficiency change as a function of gate width, while the lines labelled as 'RJ' are the SNR versus gated width. When the jitter is small, the gating efficiency increases significantly and stabilises at 100%, while a linear increase is seen when the jitter is larger than four times the pulse width. For the SNR, it decreases as the gate width becomes wider as the gate window accepts more noise counts. When the jitter is low, the SNR could be very high using a narrow gate window (sacrificing some gating efficiency), but it will decrease rapidly as the window becomes wider. However, when the jitter is very high, for instance, two or three times of the pulse width, there will not be a huge drop in SNR with increasing gate width as noise increase is balanced by increasing gating efficiency. So, once the system requirement like gating efficiency or SNR is set, or once the system jitter is characterised, then, the optimum jitter value or desired gate width could be selected based on these simulation results.

3 | JITTER SOURCE AND MATHEMATICS MODEL

To reliably detect and screen quantum signals in the presence of relative motion between the source and receiver, modulated downlink beacons are used to synchronise clocks and establish start times and thus correctly number the received quantum signals with no extra hardware. To fit within the Watt-level power budgets of the small satellites and cope with high propagation loss of up to 70 dB in the channel, the beacon is modulated into short pulsed signals with a low-repetition rate relative to the quantum signal squeezing high-peak power into the pulses to obtain sufficient SNR. In this case, the received beacon timestamps need to be interpolated to create a gating rate equal to the quantum signal repetition rate, which introduces further uncertainty. This interpolation is then deteriorated by variations in the propagation time from the satellite to the ground station caused by satellite motion varying channel length (Doppler effect) along with device imperfections and refractive index variations.

Figure 4 shows the variable noise sources suffered by the beacon and quantum signal in the propagation from the satellite to the OGS, which worsens the uncertainty between them and further degrades the SNR. The jitter mainly comes from six culprits: clock phase noise from the quantum and beacon source, atmospheric fluctuations, dark count and thermal noise in avalanche photodiodes (APD) and SPCMs, uncertainty of the arrival event time registration, non-linear variation of the signal period from the Doppler effect and the interpolation in the postprocessing. For example, the phase noise of the signal source acts directly on the synchronisation and does not leave much room for improvement; the process of the oscillator and the design of the circuit directly determine its performance. Atmospheric influences are of two kinds: turbulence causes random jitter in the optical range difference which directly deteriorates synchronisation, while refractive index changes in a slow and indirect way. In addition, the Doppler effect only introduces jitter during interpolation and is not harmful to synchronisation if the repetition rates of beacon and quantum are the same.

Figure 5 explains the interaction of different jitter sources on the signal level. The quantum signal transmitted is synchronised with a bright classical laser pulse on which the absolute index of each quantum bit is encoded using a hybrid deBruijn sequence. The receiver is able to time gate the quantum signal close to the timestamp of the beacon signal to filter most of the background noise. The top sequence is the bright beacon pulse. Due to the channel loss fluctuation, different pulses will lead to different amplitudes at the detector side which is shown in the amplitude comparison between the first and the second pulse and will introduce a discrimination error noted by J_A. Each pulse has a dashed ghosting to represent the time uncertainty of the beacon arrival marked as J_{SD}. This is normally a result of the APD thermal noise and the phase noise of the clock source. Comparing the time intervals between each two adjacent pulses, the periodic inhomogeneities marked as J_D arise from the Doppler effect of

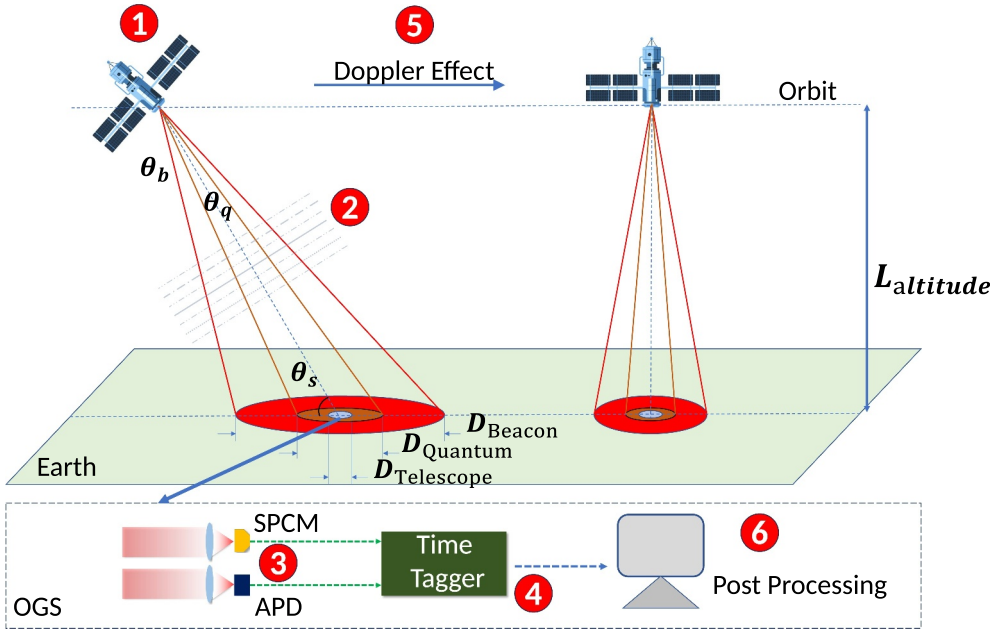

FIGURE 4 Jitter source in Free Space quantum key distribution. This is the diagram which shows the source that introduces jitter into the system. The jitter mainly comes from six sources: (1) quantum and beacon source due to the electronic thermal noise; (2) atmosphere due to the weather changing like the cloud, rain, fog, turbulence and so on; (3) detector due to the thermal noise effect on the discrimination; (4) time to digital convert sampling due to the limited digital timing resolution; (5) Doppler effect due to the non-linear period; (6) Interpolation will increase the jitter.

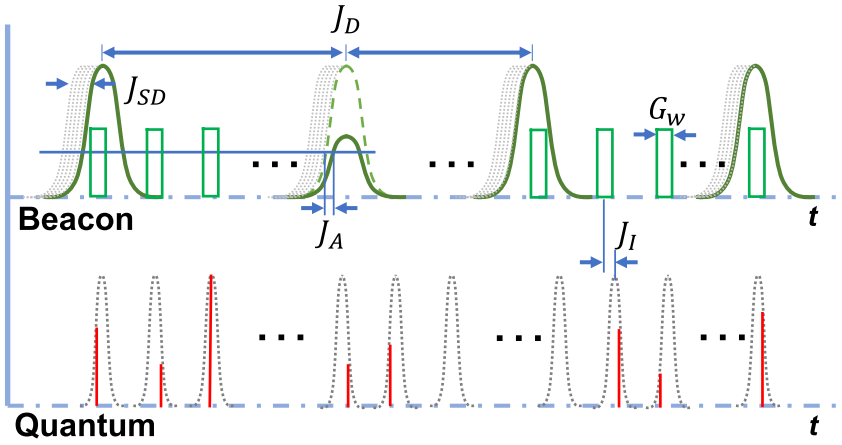

FIGURE 5 The synchronisation process of the free space quantum key distribution system. In the top flow, the dark green solid pulse is the beacon signal. The dash line shadow represents the time uncertainty resulting from the avalanche photodiodes thermal noise and the phase noise of the clock source. The time interval between the first and second pulse and between the second and third pulse is different which is introduced by the Doppler effect of the relative motion between the satellite and the ground station. The green dashed windows represent the gating window used for distilling the quantum signal out from the background noise. In the bottom flow, each dashed Gaussian pulse represents one quantum signal. The red line is the actual photon position illustrating the intrinsic jitter of the quantum signal.

relative motion between the satellite and the ground station. For low power consumption, beacons often transmit at frequencies several orders of magnitude lower than quantum signals. The selection and constraints of specific frequencies are discussed in Section 3.5. Thus, the green dash windows between each two adjacent beacon pulses are the interpolated slots used for multiplying the beacon repetition rate to synchronise the quantum signal. The gate width G_W is selected according to some factors discussed in Section 2. The bottom sequence is the quantum signal. Each grey dash pulse represents a single photon pulse in which the photon can happen at any position with a specific probability, and the red solid line is the actual photon event instant. The photon number in each pulse can be of any value and even zero, but it obeys the Poisson distribution which can be quantified using the mean photon number. J_I represents the time difference between each

gating window and the actual photon position in the time domain. The interpolation is an interesting point in the process; it does not introduce any jitter directly but can convert the different noise source into the final jitter via the practical interaction among these sources. So, figuring out the mechanism of interpolation helps us understand how different noise sources affect key generation.

According to the interaction of jitter, the total uncertainty between beacon and quantum in the QKD system is represented by Equations (1) and (2), and each noise source is analysed in detail in the following subsections, as well as providing mathematical model derivations which have been checked by the experiment.

$$sJ = \left(J_{\mathrm{SD}}^2 + J_A^2 + J_{BD}^2 + J_{QD}^2 + J_S^2\right)^{\frac{1}{2}} \tag{1}$$

$$\Delta u = I(J) + I_D(S_D) \tag{2}$$

Equation (1) shows the relationship between each jitter source and the total jitter. Where J is the total jitter, J_C is the source clock jitter, J_A is the atmospheric jitter, J_{BD} is the beacon detector jitter, J_{SPCM} is the SPCM jitter and J_S is the sampling jitter. Equation (2) gives the relationship between the system jitter and the final total uncertainty between each interpolated beacon and the corresponding quantum signal. The Δu is the total uncertainty of the system, the function $I(J)$ represents the relationship between the original jitter and the interpolated uncertainty and the function $I_D(S_D)$ shows the transformation of Doppler shifts to uncertainty where S_D is the Doppler shift introduced by the relative motion. These two functions will be derived in detail in the following subsections.

3.1 | Clock jitter

In a digital system, the piezoelectric effect is used to create a stable crystal oscillator generating a clock with specific frequency which is sensitive to the temperature. Therefore, circuit thermal noise introduced by temperature change will cause the clock frequency to randomly shift, which is called jitter. Field programmable gate arrays (FPGA's) are already used in a wide range of digital systems and are almost indispensable, especially in the field of high-speed signal processing. In order to generate clock sources with different frequencies and distribute them to the various modules of the system, phase-locked loops (PLL) are necessary to divide/multiply the input reference clock to provide the required constant frequency and to effectively isolate the input clock from jitter and drift. The PLL consists of a phase discriminator, a loop filter and a voltage controlled oscillator (VOC). Due to the temperature drift and voltage fluctuation, the VOC generates intrinsic phase noise. Based on the phase noise test, the jitter between the beacon drive clock and quantum drive clock is about 27–30 ps. The signals are output from a ZYNQ 7000 FPGA board which is used as the main controller for the payload.

3.2 | Atmospheric jitter

Atmospheric phenomena are another challenge facing QKD links including absorption, scattering and turbulence (speckle effects) of the optical signals. Relative path difference change between beacon and quantum signals with different wavelength is another contributor to the jitter. The quantum signals in between the beacon pulses also suffer from turbulence-induced timing jitter when the beacon is configured with a lower repetition to reduce the power budget. Rapid random fluctuations in the beacon pulse energy affects the pulse discrimination, thereby indirectly increasing the jitter between the signals. The fluctuation of energy is a complex problem. Absorption, scattering and spatial jitter caused by refraction will all cause fluctuation in the signal amplitude in front of the detector. The absorption of optical signals is because of the presence of water particles and carbon dioxide within the atmosphere, whereas scattering is due to fog and haze, as well as rain and snow [12, 13]. The turbulence effect has been accurately described by many distributions, including lognormal, K, I-K, negative exponential (NE), gamma, gamma–gamma (GG), Málaga (M) distribution etc., depending on the prevailing turbulence effect strength regime [14–16]. The temporal coherence time τ_0 of atmospheric turbulence is known to be in the order of milliseconds. The good news is that in a free-space QKD system, the repetition of the quantum and beacon is normally higher than 10 MHz and 10 kHz from which the turbulence is relative slow, and this gives it the possibility to compensate the jitter in the data postprocessing with a data slice width less than 1 ms. Caldwell et al. performed a measurement of the turbulence-induced optical pulse timing jitter over a horizontal, near-ground 280 m path using frequency comb lasers while independently characterising the turbulence along the path by using a suite of micrometeorological sensors; the maximum introduced jitter is within 2 ps [17]. According to the description of Equation (7) in the paper, the temporal jitter spectra is proportional to the propagation length, which means considering the Tropospheric height of 10 km, the worst case scenario is the introduction of 11.9 ps jitter. However, since there is only a very small probability that turbulence will occur over the whole channel at the same time, this value can be considered as an upper limit for the atmospheric jitter.

3.3 | Detector jitter

When the beacon arrives at the OGS after a significant attenuation, an APD is deployed to detect the signal from a noisy background which requires a high responsivity. However, the sensor itself inevitably generates a thermal electronic noise level which deteriorates the SNR. In the detector characterisation, noise equivalent power (NEP) is the input power required to reach SNR = 1 which is used for describing the intrinsic noise level and defines that the lower limit of signal power can be detected effectively. NEP is highly dependent on the bandwidth of the detector, so a trade-off usually needs to be done between them. Beyond the sensor intrinsic noise, the

amplifier and signal conditioning circuit can introduce a lot of noise. The combination will act on the signal making the signal noisy, and furthermore introduce jitter when using a discriminator to create the output clock signal, which is shown in Figure 6.

The optical pulse after high-speed modulation usually can be approximated by a Gaussian pulse leading to a similar Gaussian electronic pulse after detection. The Gaussian pulse will be discriminated by a comparator with a configured threshold voltage to be processed as digital signals from this point on. In an ideal scenario, the original signal will cross the threshold at the time $t = t_T$ which is defined as the (ideal) timestamp of this event. However, the cross point will move away from the ideal (say to $t = t_{TN}$) when the noise is superimposed on the signal. Obviously, the higher the noise at the same signal magnitude, the higher the jitter will be introduced which is also easy to understand from the point of view of SNR, and the steepness of the rising edge of the signal also affects the introduced jitter at the same noise level. To further quantify the jitter in order to provide guidance for system development and optimisation, a mathematical model is established based on this diagram.

For a common laser pulse used in most of the applications, it could be assumed that the rising edge conforms to the Gaussian waveform. So, the equation of the rise edge could be established based on the Gaussian function, as shown in Equation (3).

$$S_S(t) = A_S e^{-\frac{t^2}{2t_0^2}} (t < 0) \tag{3}$$

where A_S is the amplitude, and t_0 is the $e^{-1/2}$ half width.

Here the rise time is defined as the rising edge from 10% to 90% of the amplitude, then the relationship between t_0 and rise time t_r is established in Equations (4) and (5).

$$S_S(t_b) = 10\%, S_S(t_t) = 90\% \tag{4}$$

$$t_r = |t_t - t_b| \approx 1.61 t_0 \tag{5}$$

where t_t is the cross time at the top point (90% amplitude), and t_b is the cross time at the bottom point (10% amplitude). After combining with the noise, the signal becomes Equation (6).

$$S_S(t) = A_S e^{-\frac{t^2}{2t_0^2}} + A_n \tag{6}$$

Here, we assume that the threshold crossed time t_T is at the sharpest position of rise edge, which results in

$$\ddot{S}_S(t_T) = 0 \tag{7}$$

Then, the threshold time and the corresponding threshold are respectively

$$t_T = -t_0 \tag{8}$$

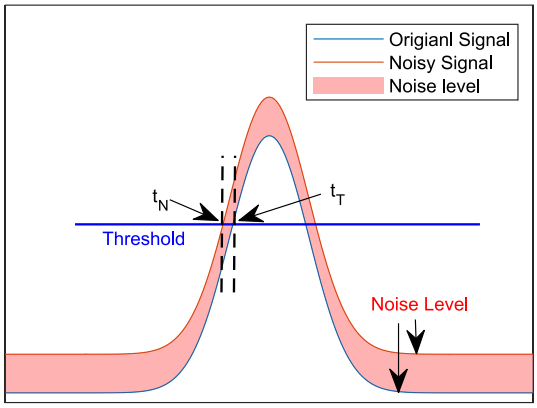

FIGURE 6 Jitter introduced by noise. A statistically root mean square (RMS) noise (red belt) superimposed on a Gaussian pulse, which crosses with the threshold (blue line) at the point t_{TN} instead of t_T. The difference between the two points results in the jitter.

and

$$A_T = A_S e^{-\frac{1}{2}} \tag{9}$$

Correspondingly, the signal superimposing the noise will cross the threshold A_T at the instant t_n.

$$t_n = -|\sqrt{2} t_0 \sqrt{-\ln\left(e^{-\frac{1}{2}} - \frac{A_n}{A_S}\right)}| \tag{10}$$

According to an empirical formula, the relationship between 3 dB bandwidth and rise time is

$$t_r = \frac{0.35}{B_w} \tag{11}$$

Finally, the time difference between the original crosspoint and practical crosspoint is the jitter introduced in the detector.

$$jitter = |-t_0 - t_n| = \frac{t_r}{1.61}\left(1 - |\sqrt{2}\sqrt{-\ln\left(e^{-\frac{1}{2}} - \frac{A_n}{P_S}\right)}|\right) \tag{12}$$

$$A_n = NEP \times \sqrt{B_w} + N_C \tag{13}$$

where the noise consists of the detector intrinsic noise $NEP \times \sqrt{B_w}$ and the post-circuit noise N_C.

Table 1 shows the specifications of two candidate APD beacon detectors: 'APD210' and 'CS13282'. The CS13282 detector from Hamamatsu has an ultra-low noise level and high responsivity compared with the APD210 from Excelitas, while the bandwidth is far lower. Figure 7 is the experiment result showing the jitter performance of the APD210 and CS13282, and both are compared with the simulation result based on the above model. The result shows that Hamamatsu's

TABLE 1 The jitter performance comparison between APD210 and CS13282.

	CS13282	APD210
Responsivity	4 MV/W	250,000 V/W
Rise time	2.7 ns	0.7 ns
NEP	0.065 pW/Hz1/2	0.4 pW/Hz1/2
Bandwidth	160 MHz	1000 MHz

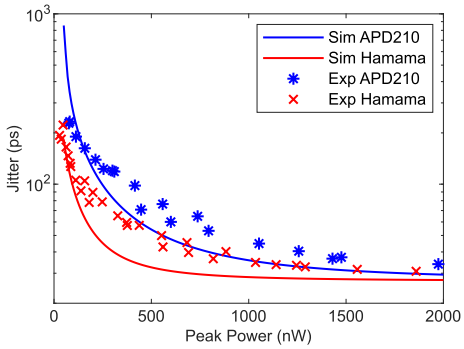

FIGURE 7 Detector jitter versus incident power determined experimentally compared to modelling. The blue asterisk data is the measured jitter of APD210, produced by Excelitas. The red cross is the measured jitter of the CS13282 from Hamamatsu. The blue (APD210) and red (Hammamatsu) solid lines show the simulation results based on the detector jitter model.

jitter is better than the APD when the incident peak power is lower than 1000 nW, after which the jitter stabilises at the same level because the SNR is high enough for both. The simulated result has a similar trend with the experiment, but the jitter levels are both lower than the practical result. This is as expected as the simulation does not introduce the exact noise level as it is hard to reach ideal performance in a practical demonstration. Moreover, the jitter stabilises to about 30 ps but not 0, this is because the incident laser pulse is driven by the FPGA, with intrinsic jitter from the FPGA which cannot be eliminated at the detector side.

3.4 | Sampling jitter

In order to record the beacon and quantum information for the postprocessing, a time to digital convert (TDC) is utilised to register the arrival time of the beacon and quantum signals. Mainstream TDCs are able to achieve ps-level resolution, which is desirable to obtain the enough accuracy of APD and PET detector in physics experiments and range finding ToF system. Precision is another specification which describes the uncertainty of time measurement, which normally results from the inconsistency of delay line units and the electronic noise. The precision highly depends on the architectures for implementing TDCs, signal conditioning and oscillator stability, which is in a range of tens to hundreds of picoseconds. In a beacon-based QKD system, the beacon and quantum signals are separately coupled into the same TDC to guarantee that they are recorded within the same time domain; thus, the increased uncertainty between the beacon and the quantum signal would be the jitter combination of two channels, $J_S = \sqrt{2}J_T$, where the J_T is the jitter of each channel of the time tagger. As the practical jitter of the TDC depends on the temperature, the EMI of the using environment and the jitter estimation should be based on the actual test.

3.5 | Doppler effect

In the vast majority of fibre-based QKD systems or station-fixed free-space QKD systems, the signal propagation time is constant because the channel distance is fixed. This is more complex in a satellite-based system as the relative motion of the satellite and OGS means the channel distance is varying. The period of the signal will change according to the relative motion viewed from the receiver, which is known as the Doppler effect. Bandpass frequency filters are used to improve the reliability of beacon detection due to the high loss of the channel and background light interference, a process made difficult by the frequency drift caused by Doppler. The thing becomes much more complex when the beacon repetition is lower than the quantum signal in order to improve the SNR with the same average power. The interpolation process will convert the time shift due to the Doppler effect into the uncertainty between the beacon and quantum channel which will contribute to the lower quantum detection efficiency. Due to the linear interpolation, the velocity component of the relative motion does not have any effect and it is the acceleration and higher order derivatives that are the main source of uncertainty as they introduce a non-linear portion into the period. In order to assess the effect of the Doppler effect on jitter, a mathematical model based on linear interpolation is developed from Equations (14)–(19), which is applicable to all cases that do not include the source's own rotation.

Assume the transmitter and the receiver are in the same time domain, and the initial distance at $t = 0$ is L. As a general case, we choose as the object of study two consecutive beacons at any moment in the process and all quantum signals in between and extend this to the whole process. The first beacon and quantum pulse are emitted at $t = 0$ and will be received by the receiver at $t_{B1} = \frac{L}{c}$. At $t = T_Q i$, the ith quantum pulse is emitted, and the distance is

$$L_i = L - \int_0^{T_Q i} v(t)dt \tag{14}$$

And it will be received at

$$t_{Qi} = T_Q \times i + \frac{L_i}{c} \tag{15}$$

The second beacon and the final quantum pulse are emitted at the same time at $t = T_B$ and the distance is

$$L_B = L - \int_0^{T_B} v(t)dt \tag{16}$$

It will be received at

$$t_{B2} = T_B + \frac{L_B}{c} \tag{17}$$

Here, we assume that $T_B = T_Q \times m$. If we use uniform interpolation, the ith interpolated pulse is at

$$t_{I_i} = \frac{t_{B2} - t_{B1}}{m} \times i + T_B \tag{18}$$

The interpolation error is defined as the difference between the actual quantum arrival time and the interpolated time, which is noted as

$$\triangle t_i = |t_{I_i} - t_{Q_i}| = \frac{1}{c}\left| \int_0^{T_Q \times i} v(t)dt - \frac{i}{m}\int_0^{T_B} v(t)dt \right| \tag{19}$$

The result, shown in Figure 8 is calculated to simulate the interpolation error introduced by the Doppler effect of a satellite in a 500 km orbit; the OGS is at a fixed site on the earth, and the max elevation angle is 90° which means the satellite will pass the OGS overhead [18]. It is clear that acceleration is increasing when the satellite is approaching the OGS and decreasing when it is flying away, thus the non-linear period change caused the acceleration peaks when the satellite passes overhead which is clear from the figure.

3.6 | Interpolation error

As mentioned above, the repetition frequency will have to be chosen as small as possible in order to achieve high peak power beacon pulses with the limited power consumption of a cube satellite. The inconsistency in repetition frequency will be compensated for by linear interpolation during the gating of the quantum signal, and this compensation will introduce more jitter due to the non-linear variation in the period generated by the beacon and the quantum signal during transmission and the increase in phase noise, which is classified here as jitter introduced by interpolation. Non-linear factors such as the Doppler effect can increase the jitter of gating due to the interpolation process, while climatic factors, such as device thermal noise, can also worsen jitter through the interpolation process. This section will model the interpolation process in order to investigate the effect of interpolation on system gating jitter and thus propose limits for each of the other noise sources.

Based on the probability theory, assume there is a clock signal with a jitter obeying the Gaussian distribution. If we consider two adjacent pulses in the clock sequence, X and Y, then,

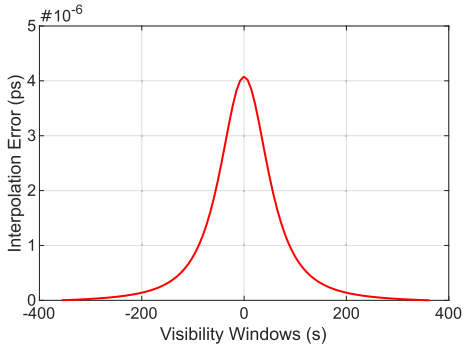

FIGURE 8 The interpolation error introduced by the Doppler effect. The result is calculated with the condition of beacon period = 10 us, orbit height = 500 km, quantum period = 100 ns and orbit inclination = pi/4.

$$X \in N\left(0, \sigma_C^2\right) \qquad Y \in N\left(0, \sigma_C^2\right) \tag{20}$$

where $N\left(0, \sigma_C^2\right)$ is the Gaussian distribution with the mean of μ and the variance of σ_C^2, the T is the ideal period of the clock signal, so the jitter of this clock is $2\sigma_C$.

When m pulses are interpolated between X and Y uniformly, the ith pulse I_C of the m pulses, which $1 \le i \le m$ is

$$I_C = \frac{Y - X}{m} \times i + X = \frac{i}{m}Y + \frac{m - i}{m}X \tag{21}$$

So the pulse I_C obeys the distribution,

$$I_C \in N\left(\frac{i}{m}T, \frac{m^2 - 2im + 2i^2}{m^2}\sigma_C^2\right) \tag{22}$$

There is another sequence of pulse which is synchronised with the clock sequence and has the same repetition with the interpolated clock sequence in which the I_d is corresponding to the I_C, and it has an uncertainty of σ_d^2. So the interpolation error is defined as follows.

$$E_I = I_d - I_C \in N\left(0, \frac{m^2 - 2im + 2i^2}{m^2}\sigma_C^2 + \sigma_d^2\right) \tag{23}$$

Due to the quantum signal and beacon signals comeing from the same clock source, $\sigma_d = \sigma_C$. The synchronised error after the interpolation is

$$std_E = \sqrt{\frac{2m^2 - 2im + 2i^2}{m^2}}\sigma_C \tag{24}$$

Here, two specific positions are discussed based on Equation (24) and also verified by the experimental result shown in Figure 9.

In the middle position, $i = \frac{m}{2}$, the error is

$$std_E(middle) = \sqrt{1.5}\sigma_C \tag{25}$$

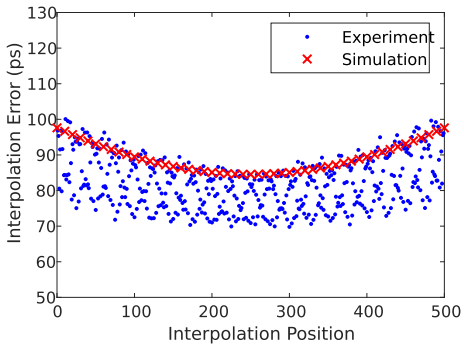

FIGURE 9 Interpolation error distribution. A 100 kHz experimental beacon sequence is interpolated to 50 MHz, with an intrinsic TIE jitter of 68 ps. The interpolated points at the same positions over many period are collected to calculate the error for that position, which is represented by the blue points. The red curve is the simulation result based on Equation (24).

Similarly, the error at side positions is

$$std_E(side) = \sqrt{2}\sigma_C \tag{26}$$

More importantly, the statistical interpolation error of a data set is derived below, which is based on the Calculus. So, the total error is

$$std_{TE}^2 = \sum_{i=1}^{m} \frac{2m^2 - 2im + 2i^2}{m^2}\sigma_C^2 \tag{27}$$

Let $dx = \frac{i}{m}$, then, the formula can be converted as an integration equation

$$std_{TE} = \sigma_C^2 \int_0^1 \frac{2m^2 - 2im + 2i^2}{m^2} dx = \sqrt{\frac{5}{3}}\sigma_C \tag{28}$$

The Equation (28) can be directly used for estimating the synchronised error after the interpolation in the scenario that the beacon and the quantum suffer the same period fluctuation in the propagation.

4 | EXPERIMENTAL DEMONSTRATION

R2.4 A proof of principle demonstration was set up based on the QKD end-to-end test bench to test the model experimentally as shown in Figure 10. The setup consists of two parts, the transmitter located on the satellite as payload and the receiver deployed on the OGS telescope. In the transmitter, the FPGA system based on the Xilinx ZYNQ 7000 worked as the central controller, used for controlling the system operation and generating the low repetition of a 100 KHz beacon trigger signal and 100 MHz random quantum trigger signal. The quantum driver drives the 785 nm quantum source to fire a 100 MHz quasi-single photon pulse with four different quantum states following the BB84 protocol [19]. The source jitter between the quantum signal and synchronised signal is about 40 ps, which was characterised by an oscilloscope. After being collimated by the focus lens, the beam passed through a beam splitter (BS) with a portion of the signal reflected into an optical powermeter to monitor the quantum source power. In the beacon channel, a bright 904 nm beacon pulse train was emitted driven by a high-power laser driver based on eGaN FET EPC2001C, whose peak power could be up to 125 W with 4.1 ns pulse width and 100 KHz repetition. After collimation by the lens, it passed through the same aperture as the quantum signal. A ND filter was mounted after the aperture to simulate the fixed loss portion in the communication link, while a motorised polariser was located after that to simulate the variable channel loss during the satellite scientific pass.

In the receiver, a long-pass dichroic mirror was used to separate the beacon, and the quantum channel and bandpass filters (785 nm and a 905 nm, respectively) were mounted in front of the two channels to block background light and improve the SNR. The quantum signals were coupled into SPCMs based on the polarisation feature to be converted into an electronic signal. The beacon was also detected by a high responsivity APD, but the post-processing is more complex. To compensate the amplitude change resulting from variable channel loss, a constant fraction discriminator was designed after the APD which converts the simple Gaussian pulse into an intensity-insensitive signal so that a constant threshold will introduce less jitter. The attenuated beacon was focused onto the APD detector and converted to an electronic signal. Finally, both quantum and beacon signals were registered by a time tagger, and the tags were processed by the analyser. The jitter of a time tagger is around 80 ps, which is consistent with the actual device used in the future mission.

In the experiment, a series of beacon signals with different channel losses and different repetition frequencies were generated to investigate the respective effects on signal jitter. On this basis, the jitter of the collected signals was fed into the interpolation model developed in Section 3, which was used to calculate the theoretical interpolation error and to compare it with the actual interpolated statistical error, thus verifying the correctness of the model. To remove the effects of channel loss differences, and jitter differences and quantum efficiency differences in SPCMs, only one quantum state channel was used for data acquisition in the experiments, and the independence of the jitter levels of each quantum state ensured that this choice does not affect the results. Considering the limitations for the quantitative generation of Doppler effect and atmospheric conditions, here, we used simulated data and input them into the interpolation model for the study.

4.1 | Interpolation error versus loss and repetition

To illustrate the channel loss effect on jitter described in the detector jitter section, a range of different channel losses were configured via a variable ND Filter in the transmission channel

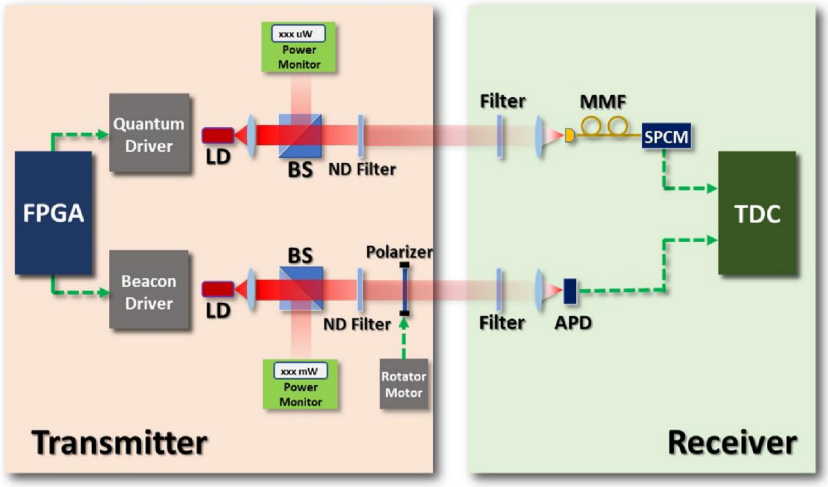

FIGURE 10 Test bench for studying the jitter effect on the quantum detection. The testbench is made of two parts, the transmitter and the receiver. In the transmitter, a 785 nm BB84 quantum source and a 905 nm beacon clock source are synchronised by the main controller field programmable gate arrays, The quantum mean photon number is lower than $\mu = 0.1$ and there is another ND filter mounted to simulate the channel loss. The beacon passes through a rotated linear polariser which can modulate the beacon power automatically. The receiver includes a photon counting quantum receiver and the linear mode beacon avalanche photodiodes, which are connected to separate channels of the time tagger.

to obtain corresponding jitter results. In addition, considering that the repetition rate determines the power budget for a given pulse energy, jitter due to Doppler non-linear effects at different repetition frequencies is also explored, which can be used to provide a reference for engineering design. For the LEO satellite, the visibility window is about 10 min according to the orbit height, and the maximum distance is up to 1700 km at 10°, so the channel loss changes in the range from 41.7 to 52.3 dB.

Figure 11 shows the experimental results looking at how jitter between the quantum signal and the synchronising beacon changes with a different beacon repetition rate and the loss before the interpolation. The jitter was calculated using the time interval between each beacon and the corresponding quantum one, after which the SPCM jitter and quantum pulse width were removed so that the final result is independent of them.

When the channel loss is lower than 60 dB, the jitter is staying around 140 ps, after which the value increases exponentially and reach to 340 ps at 80 dB. The time tagger contributes 100 ps jitter to the total value. The detected beacon power change only affects the detector jitter, so when the detector jitter is non-dominant, the change can be ignored and the total jitter maintained to 140 ps. However, the beacon detector becomes a dominant contribution to the total jitter for a loss greater than 60 dB. For the repetition rate, it is obvious that the jitter trend with loss is similar under different rates, but a higher rate would result in a worse jitter. This is mainly because the peak power of the beacon pulse drops as the repetition rate increases. The principle of operation of the beacon driver is based on a resistor, inductor, capacitor resonant topology, and a higher repetition means there is less time for the recharging loop to recharge the energy to the capacitors which results in a lower intensity pulse. So a lower repetition

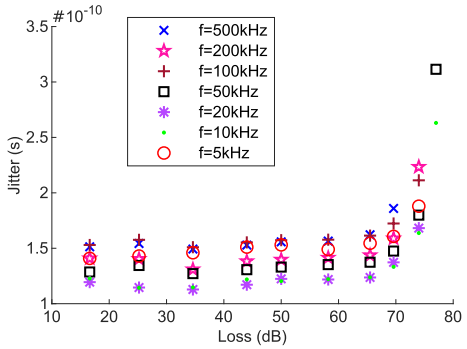

FIGURE 11 Beacon discrimination jitter plotted against loss at various repetition rates. The beacon repetition is configured to different values from 5 to 500 kHz while keeping the same pulse peak power, and the quantum repetition is 100 MHz. Due to the optical pulse intensity variation resulting from the driver recovery between pulses, the beacon discrimination jitter does change at different repetition rates. Generally, jitter increases with loss particularly above 60 dB with the plot extending up to 80 dB to cover the maximum channel loss in a real scenario. This jitter also includes the jitter from the time tagger which is about 80 ps.

frequency of the beacon is more desirable in terms of peak power and average power consumption.

Figure 12 shows the comparison between the experimental interpolation error and the calculated interpolation error. In the experiment, beacon pulses with different repetitions are captured by the time tagger. The jitter is calculated with the registered time tags, and the corresponding interpolation error is simulated which is shown with the asterisks in the figure. Then, the interpolation is performed, and the error is directly estimated, which is shown as circles in the figure. They have a same change trend with the channel loss increasing, but the errors obtained by actual interpolation are relatively higher at different repetition rates compared with simulated result.

4.2 | Gating efficiency versus jitter

To verify the effect of clock jitter on gated quantum signals as described in Section 2, a series of gating experiments is done under different clock jitter. In the experiment, the quantum key rate is 25 MHz while the detected photodetection count rate is around 400 kHz after the channel attenuation. The beacon is modulated at 100 KHz and passes through a rotated polariser and a ND filter. The loss can be configured by rotating the linear polariser (the beacon source is linearly polarised), thus the detection jitter of APD will be changed correspondingly. The beacon discrimination jitter is controlled between 150 and 700 ps to collect quantum tags and calculate the gating efficiency. The gate window width is configured as 1 ns, while the full width half maximum (FWHM) of the quantum signal distribution is 900 ps.

As shown in the Figure 13, the quantum gating efficiency is decreasing linearly with the increase of the beacon clock jitter, or we say the signal to noise ratio decreases when the beacon clock jitter increases. The trend is linear as the jitter range is small compared with the FWHM of the quantum signal distribution.

4.3 | Doppler effect versus repetition rate

The power budget of small satellites becomes very tight due to size constraints, and it becomes very important to use less power to achieve the appropriate performance. From the digital coding point of view, the choice of the reference signal clock frequency will have no effect on the synchronisation results, only the need to interpolate over different ranges accordingly, but a lower frequency can significantly reduce the average optical power required by the system. However, according to the Doppler interpolation model presented above, a low frequency clock leads to an increase in the drift of each clock, which leads to an increase in the jitter of the interpolated synchronisation pulse, reducing the filtering ability of the noise as well as the signal selection ability. To figure out the practical influence of the Doppler effect on the interpolation error, the Doppler effect jitter under different repetition rates during the scientific pass is simulated as shown in the Figure 14. From the figure, we can see that during the satellite pass, when the repetition is higher than 1 kHz, the jitter introduced is always under 1 ps which has a negligible effect on the overall jitter. However, once the repetition is lower than the threshold, the jitter is increased significantly which will deteriorate the clock performance. Besides, the interpolation error increases as the inverse square of the repetition frequency, which means, when the beacon period decreases from $TB = 1e-1$s to $TB = 1e-2$s, the error difference between the green line and purple line increases $\times 10^2$. Of course, the repetition rate is also constrained by the average power siphoned off pointing and tracking and the polarisation analyser. So this result gives

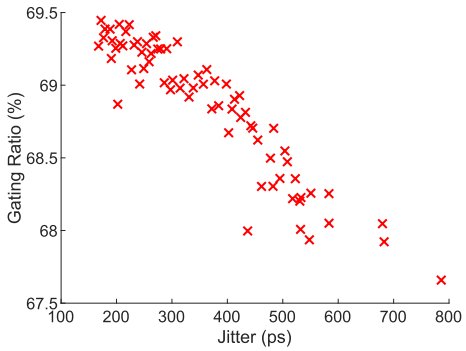

FIGURE 13 Quantum tags gating efficiency with different beacon discrimination jitter. The mean photon number is 0.1, and the channel loss is 8 dB. The time tagger's intrinsic jitter is 100 ps.

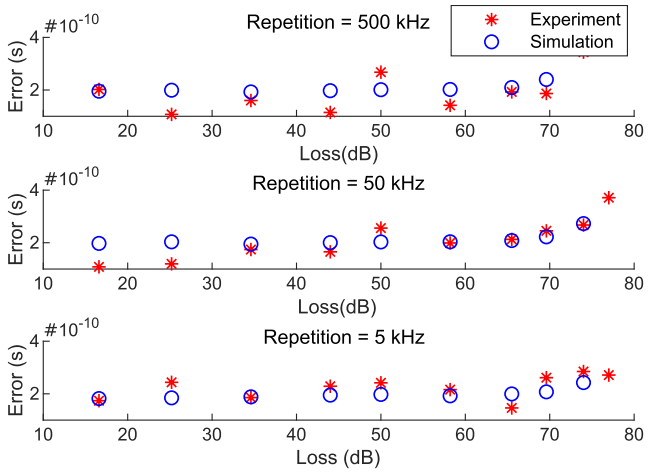

FIGURE 12 Interpolation error against loss and repetition. The interpolation error collected via experiments and simulation is compared with different repetition rates. The red asterisks represent the results derived from the interpolation experiments, and the blue circle represents the results of the interpolation simulation based on the beacon jitter. They agreed with each other within the range of 10–80 dB channel loss and show the same 'exponential like' increase above 60 dB loss.

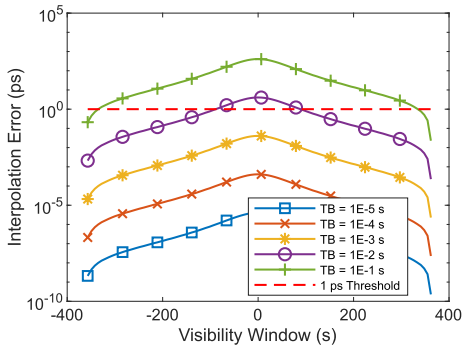

FIGURE 14 Doppler Effect under different repetition. The figure shows the interpolation error variation when the LEO satellite (500 km) is within the view of the optical ground station. From top to bottom, the error corresponds to a beacon period of 100 ms, 10 ms, 1 ms, 100 us and 10 us. The red dash line is the baseline, and all the data points above it represent errors larger than 1 ps.

the lower bound of the repetition selection in the low-orbit payload application.

5 | CONCLUSIONS

In this study, we proposed a mathematical model to study how the noise source affects the key generation of a free space QKD system. The model firstly discusses the clock jitter effect on the detection efficiency of quantum signals, and it shows that when the jitter value is equal to or even greater than the half-height width of the signal, the detection efficiency of the signal will be significantly reduced. Then, the model analyses the jitter sources in a free space QKD system, describing the contribution of the different noise sources to jitter and focuses on the detailed mathematical analysis of detector, Doppler effect and interpolation noise jitter. A corresponding set of experimental jitter measurements were carried out, and the results are consistent with the theoretical analysis. The effect of uniform interpolation on signal jitter is modelled and verified by multiple interpolation experiments. The results show that the interpolation process increases the jitter of the clock and tends to be low in the middle and high on both sides. The jitter introduced by the Doppler effect is modelled, and the simulation results agree with the mathematical calculations. The results show that by choosing a clock signal with a repetition frequency higher than 1Khz, it is possible to ensure that the jitter of the Doppler effect does not have any measurable impact on the system performance.

This work characterises the effect of clock jitter on the efficiency of quantum detection in QKD systems by building mathematical models and systematically analyses the sources and magnitudes of clock jitter in the overall system. The findings can be directly applied to the design and optimisation and performance evaluation of satellite and ground station-based QKD systems, as well as to any QKD system containing the subsystems or devices described.

AUTHOR CONTRIBUTIONS

Peide Zhang: Conceptualisation; data curation; formal analysis; investigation; methodology; resources; software; validation; visualisation; writing – original draft; writing – review & editing. **David Lowndes**: Conceptualisation; investigation; methodology. **Milan Stefko**: Resources. **Daniel Oi**: Conceptualisation; investigation; methodology; supervision; writing – review & editing. **John Rarity**: Conceptualisation; funding acquisition; investigation; methodology; project administration; resources; supervision; writing – review & editing.

ACKNOWLEDGEMENTS

This research was funded by the EPSRC Quantum Communications Hub (EP/T001011/1) and the UK Space Agency (NSTP3-FT2-065 QSTP: Quantum Space Technology Payload, NSIP-N07 ROKS Discovery). The first author was supported by the University of Bristol—China Scholarship Council joint-funded Scholarship to participate in this research. DO is supported by the EPSRC (EP/T517288/1) and acknowledges discussions with S. K. Joshi.

CONFLICT OF INTEREST STATEMENT

The authors declare no conflicts of interest.

DATA AVAILABILITY STATEMENT

Data available on request from the authors.

ORCID

Peide Zhang https://orcid.org/0000-0003-4595-8151
Daniel Oi https://orcid.org/0000-0003-0965-9509

REFERENCES

1. Liao, S.K., et al.: Satellite-to-ground quantum key distribution. Nature 549(7670), 43–47 (2017). https://doi.org/10.1038/nature23655
2. Bedington, R., Arrazola, J.M., Ling, A.: Progress in satellite quantum key distribution. NPJ Quan. Inf. 3(1), 30 (2017). https://doi.org/10.1038/s41534-017-0031-5
3. Calderaro, L., et al.: Fast and simple qubit-based synchronization for quantum key distribution. Phys. Rev. Appl. 13(5), 054041 (2020). https://doi.org/10.1103/physrevapplied.13.054041
4. Wang, C.Z., et al.: Synchronization using quantum photons for satellite-to-ground quantum key distribution. Opt Express 29(19), 29595–29603 (2021). https://doi.org/10.1364/OE.433631
5. Batori, E., et al.: GNSS-grade space atomic frequency standards: current status and ongoing developments. Adv. Space Res. 68(12), 4723–4733 (2020). https://doi.org/10.1016/j.asr.2020.09.012
6. Shen, Q., et al.: Pulsed optically pumped atomic clock with a medium- to long-term frequency stability of 10^{-15}. Rev. Sci. Instrum. 91(4), 045114 (2020). https://doi.org/10.1063/5.0006187
7. Wang, C., et al.: Robust aperiodic synchronous scheme for satellite-to-ground quantum key distribution. Appl. Opt. 60(16), 4787–4792 (2021). https://doi.org/10.1364/AO.425085
8. Agnesi, C., et al.: Sub-ns timing accuracy for satellite quantum communications. JOSA B 36(3), B59–B64 (2019). https://doi.org/10.1364/josab.36.000b59
9. Zhang, P., et al.: Timing and synchronisation for high-loss free-space quantum communication with Hybrid de Bruijn Codes. IET Quan. Commun. 2(3), 80–89 (2021). https://doi.org/10.1049/qtc2.12019
10. Berra, F., et al.: Synchronization of quantum communication over an optical classical communication channel. (2023). https://doi.org/10.48550/arXiv.2306.17603
11. Belenchia, A., et al.: Quantum physics in space. Phys. Rep. 951, 1–70 (2022). https://doi.org/10.1016/j.physrep.2021.11.004
12. Popoola, W.O., et al.: Scintillation effect on intensity modulated laser communication systems—a laboratory demonstration. Opt Laser. Technol. 42(4), 682–692 (2010). https://doi.org/10.1016/j.optlastec.2009.11.011
13. Gripeos, P.J., et al.: Time and spatial jitter influence on the performance of FSO links with DF relays and OC diversity over turbulence channels. Photonics 8(8), 318 (2021). https://doi.org/10.3390/photonics8080318
14. Mahdieh, M., Pournoury, M.: Atmospheric turbulence and numerical evaluation of bit error rate (BER) in free-space communication. Opt Laser. Technol. 42(1), 55–60 (2010). https://doi.org/10.1016/j.optlastec.2009.04.017
15. Zhang, B., Yan, H.: The internal-collision-induced magnetic reconnection and turbulence (ICMART) model of gamma-ray bursts. Astrophys. J. 726(2), 90 (2010). https://doi.org/10.1088/0004-637X/726/2/90
16. Picozzi, A., Garnier, J.: Incoherent soliton turbulence in nonlocal nonlinear media. Phys. Rev. Lett. 107(23), 233901 (2011). https://doi.org/10.1103/PhysRevLett.107.233901
17. Caldwell, E.D., et al.: Optical timing jitter due to atmospheric turbulence: comparison of frequency comb measurements to predictions from

micrometeorological sensors. Opt Express 28(18), 26661–26675 (2020). https://doi.org/10.1364/OE.400434
18. Ali, I., Al-Dhahir, N., Hershey, J.: Doppler characterization for LEO satellites. IEEE Trans. Commun. 46(3), 309–313 (1998). https://doi.org/10.1109/26.662636
19. Bennett, C., Brassard, G.: Quantum cryptography: public key distribution and coin tossing. Theor. Comput. Sci. 560, 175–179 (1984). https://doi.org/10.1016/j.tcs.2014.05.025

How to cite this article: Zhang, P., et al.: Modelling and experimental testing of an optical synchronisation beacon designed for high-loss satellite quantum communication. IET Quant. Comm. 1–14 (2023). https://doi.org/10.1049/qtc2.12071